SIAM J. APPL. MATH.
Vol. 62, No. 1, pp. 206–225

SPATIALLY STRUCTURED ACTIVITY IN SYNAPTICALLY COUPLED NEURONAL NETWORKS: I. TRAVELING FRONTS AND PULSES*

DAVID J. PINTO† AND G. BARD ERMENTROUT‡

Abstract. We consider traveling front and pulse solutions to a system of integro-differential equations used to describe the activity of synaptically coupled neuronal networks in a single spatial dimension. Our first goal is to establish a series of direct links between the abstract nature of the equations and their interpretation in terms of experimental findings in the cortex and other brain regions. This is accomplished first by presenting a biophysically motivated derivation of the system and then by establishing a framework for comparison between numerical and experimental measures of activity propagation speed. Our second goal is to establish the existence of traveling pulse solutions using more rigorous methods. Two techniques are presented. The first, a shooting argument, reduces the problem from finding a specific solution to an integro-differential equation system to finding any solution to an ODE system. The second, a singular perturbation argument, provides a construction of traveling pulse solutions under more general conditions.

Key words. synaptic networks, cortical activity, wave speed, shooting method, singular perturbation

AMS subject classification. 92C20

PII. S0036139900346453

1. Introduction.

Analysis of the mechanisms underlying spatially structured activity in neural tissue is important for understanding a wide range of both naturally occurring and pathological phenomena. In sensory cortex, horizontal connections may serve to bind responses to related sets of stimuli, allowing them to be processed and perceived as a single unit [56], [25]. In the turtle visual cortex, the presentation of stimuli has been shown to evoke propagating waves of activity [45]. Neurological disorders in humans such as epilepsy and migraine are also characterized by traveling activity waves propagating across the surface of the brain [8], [39]. Similar phenomena are often studied in animal models by pharmacologically blocking inhibitory synaptic activity (e.g., [61], [8], [7]).

A common experimental paradigm for the study of neuronal waves is to record activity in vitro using a thin brain slice preparation (e.g., [61], [7]). While much of the complexity of whole-brain waves is undoubtedly lost as compared to in vivo experiments, in vitro preparations are more amenable to pharmacological manipulation and spatial recording of neuronal activity. In the addition, the relationship between spatially structured activity and the underlying neuronal circuitry that supports it is likely to be more straightforward and easier to understand in a reduced biological model.

The analysis of spatial activity can also be facilitated by considering the synaptic architecture of specific brain regions. In the mammalian neocortex, for instance, connectivity patterns follow a laminar arrangement with strong vertical coupling between layers [58]. For this reason, spatial activity in cortex is often considered as occurring

*Received by the editors July 5, 2000; accepted for publication (in revised form) March 2, 2001; published electronically August 22, 2001. This work was supported by grants from NSF, NIMH, and NIH.

http://www.siam.org/journals/siap/62-1/34645.html

†Department of Neuroscience, Brown University, Providence, RI 02912 (dpinto@bu.edu).

‡Department of Mathematics, University of Pittsburgh, Pittsburgh, PA 15261 (bard@pitt.edu).

on a two-dimensional plane with the coupling between layers making vertical propagation nearly instantaneous. The phenomena can be simplified further by using a brain slice preparation taken across cortical layers so that wave-like activity is effectively constrained to a single dimension. Figure 1(a) shows a typical "across-layer" cortical brain slice and the marks left behind by a line of recording electrodes placed along a single layer. Figure 1(b) shows a traveling activity wave recorded from those electrodes when synaptic inhibition is pharmacologically blocked. (See Appendix for methods.)

In the present study we consider traveling solutions of an integral equation used to describe the activity of a synaptically coupled neuronal network in a single spatial domain:

$$u(x,t) = \int_{-\infty}^{\infty} w(x-x') \int_{-\infty}^{t} \alpha(t-t') P(u(x',t') - \theta) dt' dx'. \tag{1}$$

Note that, in the case of $\alpha(t) = e^{-t}$, (1) can be equivalently expressed as

$$u_t(x,t) + u(x,t) = \int_{-\infty}^{\infty} w(x-x') P(u(x',t) - \theta) dx'. \tag{2}$$

Here, u is taken to be the average activity (e.g., voltage) level of a neuronal population at spatial point x and time t, w is the distance-dependent strength of connectivity between neuronal populations, α is the time course of activity resulting from a single synaptic event, and P is the synaptic firing rate, which depends on the level of activity, u, relative to some threshold value, θ. (See [13] for a review.)

In section 2, we establish a series of direct links between the abstract model equations and their interpretation in terms of experimental findings in neocortex. Each component of the equation is described both mathematically and in terms of its correspondence to features of neocortical circuitry. We then explore both analytically and numerically the relationship between those components and the speed of front propagation, an experimental measure relatively easy to obtain in the laboratory. These results extend the work of [18] and [6], establishing the existence and uniqueness of traveling front solutions to (1), e.g., solutions of the form $u(x,t) = U(x-ct)$, monotonic decreasing, $U(-\infty) = 1$, $U(\infty) = 0$, $U(0) = \theta$, and c of constant value.

In the neuronal tissue, propagating activity does not persist indefinitely but rather is transient in nature. Even in the absence of synaptic inhibition, most neurons possess intrinsic negative feedback mechanisms that slowly bring the cell back to resting voltage levels following periods of high activity [38]. Rather than a traveling front, propagating activity in the brain is better described as a traveling pulse. We incorporate a recovery mechanism into the equations with the addition of a slow, local negative feedback component, v, added to the synaptic spatial coupling described by (2):

$$\begin{aligned} u_t(x,t) + u(x,t) &= \int_{-\infty}^{\infty} w(x-x') P(u(x',t) - \theta) dx' - v(x,t), \\ \frac{1}{\epsilon} v_t(x,t) + \beta v(x,t) &= u(x,t), \qquad \epsilon \ll 1. \end{aligned} \tag{3}$$

This negative feedback could represent spike frequency adaptation, synaptic depression, or some other slow process that limits the excitation of the network. Figure 1(c) presents a numerical example of a traveling pulse solution to (3). (See Appendix for methods.)

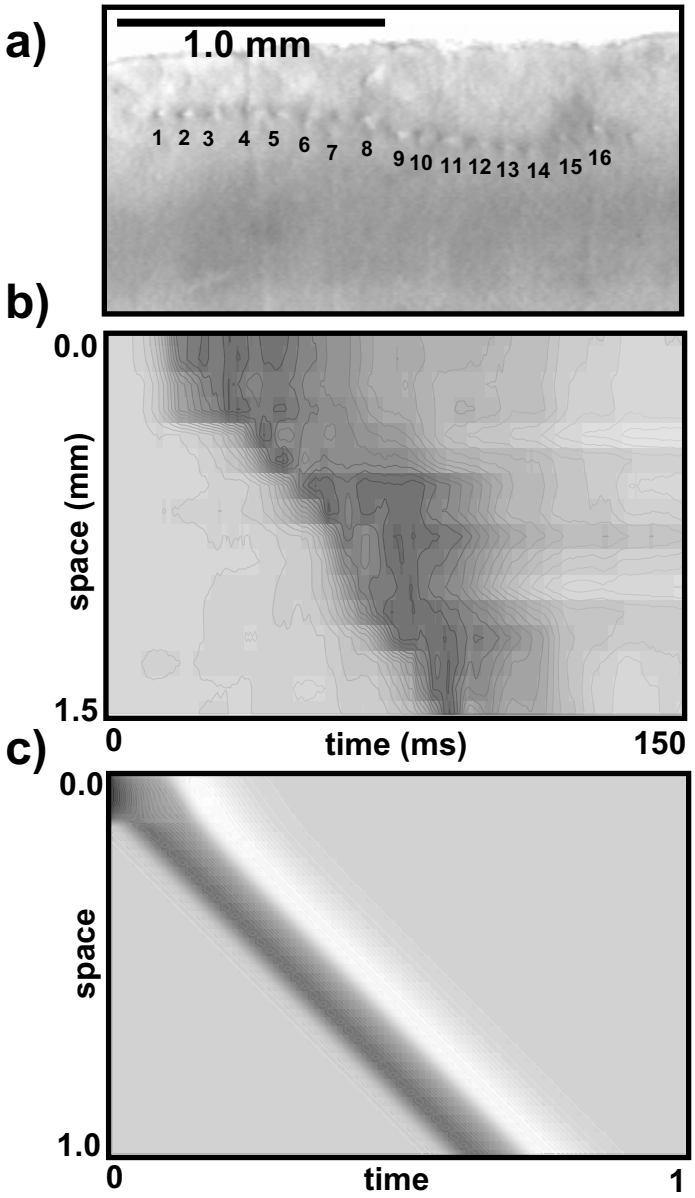

FIG. 1. *Real and simulated traveling pulses.* (a) *A thin-slice brain section through rodent somatosensory cortex. Small numbers denote marks left behind by an array of* 16 *extracellular field potential electrodes placed along cortical layer* II/III *parallel to the pial surface. Interelectrode spacing is* .1 *mm.* (b) *An example of a traveling activity pulse induced by pharmacologically blocking synaptic inhibition and applying a brief (*.2 *ms) stimulus left (*.5 *mm) of electrode* #1. *Data from each of the* 16 *electrodes is presented along the vertical axis. Time is represented on the horizontal axis. Darker shades of gray denote high levels of neuronal activity.* (c) *A traveling pulse obtained numerically from the model system described by* (2) ($\theta = .25, \tau = .15$). *No attempt was made to rescale time and/or space to match the simulations with real data. (See Appendix for methods.)*

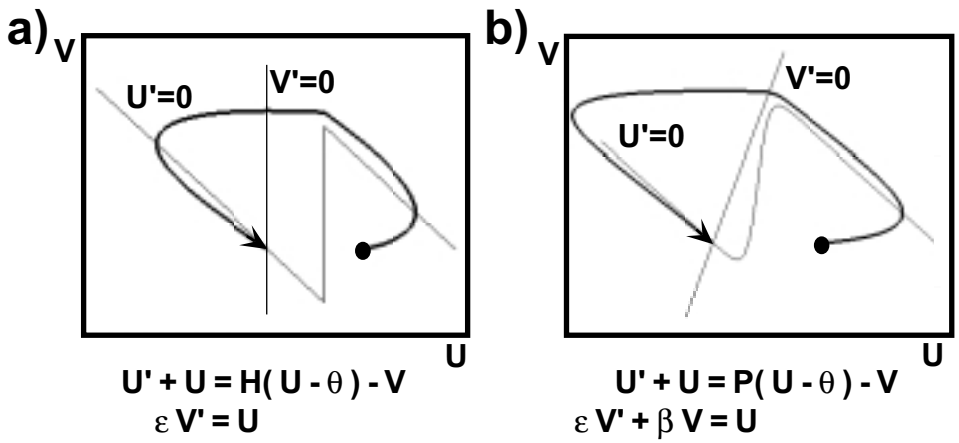

FIG. 2. *Local phase-plane analysis of traveling pulse dynamics. For the shooting argument* (a) *(section* 3.1*), the local dynamics are restricted but display the same essential features as the general case* (b) *(section* 3.2*).*

In section 3, we establish the existence of traveling pulse solutions to (3) using more rigorous techniques. The first approach, a shooting argument, considers the specific case in which the decay of negative feedback is weak (i.e., $\beta = 0$), and the firing rate, P, is described using the Heaviside function. The second approach, a singular perturbation argument, considers the more general system and exploits the difference in time scales introduced by slow negative feedback.

The intuitions behind both methods can be understood by considering their "space-clamped" phase-planes (see Figure 2). In each case, the intersection of a linear "inhibitory" nullcline with the right branch of an "N"-shaped "excitatory" nullcline results in a single, stable equilibrium point. By raising the activity at one location above threshold, the excitable dynamics and network connections lead to above-threshold activity in neighboring regions. The wave of activity terminates at each spatial point as slow negative feedback carries the local system back to its rest state. For the shooting argument (Figure 2(a)), the additional assumptions restrict local dynamics but also, as described in section 3.1, enable the problem to be reduced from finding a *specific* solution of an integro-differential equation to finding *any* solution of an ODE. For the singular perturbation argument (Figure 2(b)), the local dynamics are more general, but, as described in section 3.2, the ability to construct solutions is, at present, restricted to asymptotic approximations.

2. Biological relevance. We begin with a detailed presentation of the equation describing spatial activity in a neocortical slice, interpreting each component in terms of specific features of cortical circuitry. We then analyze the wave solutions in order to capture the relationship between each component and the speed of propagation.

2.1. Deriving the equations. Interactions between synaptically coupled neurons occur via all-or-none events called action potentials. A single action potential evokes a voltage change, or a postsynaptic potential (PSP), in the postsynaptic element. PSPs follow characteristic time courses that depend on both synaptic and membrane time constants and are typically described using "alpha" functions, $\alpha(t)$ [46]. For the analysis below, we require $\alpha(t)$ to be defined on $[0, \infty)$, monotonic decreasing, nonnegative, and normalized such that $\int_0^\infty \alpha(t)dt = 1$. As a particular

example, consider $\alpha(t) = \frac{1}{d}e^{-t/d}$, where $1/d > 0$ represents the decay rate. Numerical results are also presented using the more general double exponential form,

$$\alpha(t) = \frac{e^{-t/d_1} - e^{-t/d_2}}{d_1 - d_2},$$

where d_1 is related to the synaptic rise time and d_2 to the decay rate. Taking the limit as $d_1 \to d_2$, this approaches $\alpha(t) = te^{(-t/d_2)}/d_2^2$, often used as the standard definition for $\alpha(t)$ [46]. For $\alpha(t)$ in this form, however, the necessary existence results employed below have not yet been rigorously established.

For a series of n action potentials, alpha functions summate, and the voltage level, u, in the postsynaptic neuron is given by

$$u(t) = w \sum_{i=1}^{n} \alpha(t - t_i),$$

where t_i is the time of occurrence for each of the n action potentials, and w is a positive scaling term describing the strength of the synaptic interaction. Note that, with $\alpha(t)$ normalized, the strength or "weight" of the synapse is described entirely by the scaling parameter w.

Considering a population of neurons, and assuming that the individual neuronal firing times are uncorrelated [24], the distribution of action potentials over time can be described using a continuous, saturating function, $P(u(t) - \theta)$, indicating the average instantaneous firing rate within the population. Intuitively, the shape of P is determined both by the active processes involved in action potential generation [14] and by heterogeneities among the neurons in the population [44], [24]. Also, $u(t)$ is now taken to represent the average population voltage level, and θ is some constant threshold value ($0 < \theta < 1$). We require the function $P(u)$ to be defined on $[0, 1]$, monotonically increasing, $P'(0) < 1$, $P'(1) < 1$, and such that the function $f(u) \equiv -u + P(u)$ has precisely three zeros, typically at or near $u = 0$, ξ, and 1 with $0 < \xi < 1$. As a particular example, consider $P(u - \theta) = \frac{1}{2}(1 + \tanh(\beta(u - \theta)))$, or, as a limiting case ($\beta \to \infty$), $P(u - \theta) = H(u - \theta)$, where $H(x) = 0$ for $x < 0$, $H(x) = 1$ for $x \geq 0$. The average population voltage level is then described by

$$u(t) = w \int_{-\infty}^{t} \alpha_e(t - t')P_e(u(t') - \theta)dt'.$$

Extending into the spatial domain, a continuum of local populations can be considered, with synaptic strengths described by a spatial distribution of weights,

$$u(x,t) = \int_{-\infty}^{\infty} w(x - x') \int_{-\infty}^{t} \alpha(t - t')P(u(x', t') - \theta)dt'dx'. \tag{4}$$

Rather than actual location, weight distributions are typically expressed in terms of the distance between locations. We require the function w to be defined on $(-\infty, \infty)$, bounded, nonnegative, even, and normalized such that $\int_{-\infty}^{\infty} w(x)dx = 1$. As a particular example, consider $w(x) = e^{-|x|/b}/2b$ or $w(x) = 2\sqrt{b/\pi}e^{-bx^2}$, where $b > 0$ describes the width of the synaptic "footprint."

2.2. Wave speed. Relatively simple to determine experimentally, the measure of wave speed incorporates many features of the underlying circuitry and provides a

useful probe into the mechanisms of wave propagation. Several recent studies have explored, both numerically (see [26], [40], [54]) and analytically (see [3], [26], [12], [33], [18]), the relationship between network model parameters and wave speed in various settings. Here, we exploit the simple form of the present model to quantitatively characterize the relationship between wave speed and firing threshold, synaptic parameters, and axonal conduction velocity. Using a conductance based variation of the model, we illustrate the relationship between wave speed and intrinsic and synaptic conductances. Finally, numerical results are presented that compare analytic results with simulation, illustrating the significance of nonlinearities in the firing rate function for determining speed. A subsequent report will examine experimentally the relationship between wave speed and various circuit components and compare the results to those presented here (D.J. Pinto and B.W. Connors, in preparation).

2.2.1. Speed, threshold, footprints, and decay. Assuming a traveling front solution to (1), $U(x-ct)$ with $U(-\infty)=1$, $U(\infty)=0$, $U(0)=\theta$, and with the Heaviside function, $H(u-\theta)$, describing firing rate, a series of substitutions may be employed to obtain an implicit function of wave speed in terms of the various parameters. Beginning with the equation describing the solution,

$$U(x-ct)=\int_{-\infty}^{t}\alpha(t-t')\int_{-\infty}^{\infty}w(x-x')H(U(x'-ct')-\theta)dx'dt',$$

we express space in terms of traveling coordinates ($z=x-ct$, $z'=x'-ct'$) and time in terms of past time ($s=t-t'$),

$$\begin{aligned}U(z)&=\int_{0}^{\infty}\alpha(s)\int_{-\infty}^{\infty}w(z+cs-z')H(U(z')-\theta)dz'ds\\&=\int_{0}^{\infty}\alpha(s)\int_{-\infty}^{0}w(z+cs-z')dz'ds.\end{aligned}$$

Then we substitute the integration variables $r=z/c+s$ and $y=cr-z'$,

$$U(z)=\int_{\frac{z}{c}}^{\infty}\alpha\left(r-\frac{z}{c}\right)\int_{cr}^{\infty}w(y)dydr,$$

and evaluate at $z=0$,

$$\theta=\int_{0}^{\infty}\alpha(r)\int_{cr}^{\infty}w(y)dydr, \tag{5}$$

to arrive at a straightforward expression describing the influence of various parameters on wave speed.

Figure 3 illustrates the effect on wave speed of the firing threshold, θ, synaptic footprint, b, and synaptic decay rate, d. At each threshold value, both wide synaptic footprints (Figure 3(a)) and faster synapses (Figures 3(b) and 3(c)) result in faster waves. Figure 3(c) reveals a similar relationship between wave speed and synaptic decay using more realistic synaptic dynamics. Note that, in each case, wave speed $c=0$ occurs just when $\theta=.5$. The symmetry of speeds between high- and low-threshold values arises from the symmetry of the weight distributions and firing rate functions.

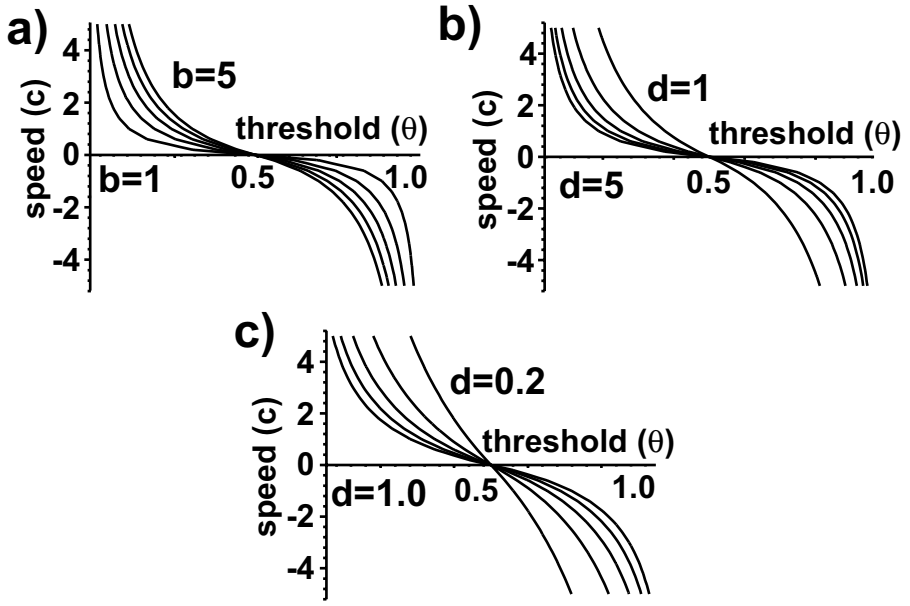

FIG. 3. *Effect on wave speed of firing threshold, synaptic footprint, and synaptic decay rate. The relationship between wave speed (c) and firing threshold (θ), synaptic footprint (b), and synaptic decay rate (d) is described by,* $\theta = \int_0^\infty \frac{1}{d} e^{-\frac{s}{d}} \int_{cs}^\infty \frac{1}{2b} e^{-|y|/b} dy ds$ *(i.e.,* (5)*). Note that, in each case, zero wave speed occurs just when* $\theta = .5$. (a) *Increasing synaptic footprints results in faster wave speeds* ($d = 3$, $b = 1, 2, 3, 4, 5$). (b) *Fast-acting synapses also act to increase wave speed* ($b = 3$, $d = 1, 2, 3, 4, 5$). (c) *The relationship between wave speed and synaptic decay is similar using more realistic synaptic dynamics* ($b = 3$, $\alpha(t) = \frac{t}{d^2} e^{(\frac{t}{d})}$, $d = .2, .4, .6, .8, 1.0$).

2.2.2. Wave speed and conduction velocity. We incorporate axonal conduction velocity into (2) by delaying the influence of activity from other regions based on their distance, i.e.,

$$u_t(x,t) + u(x,t) = \int_{-\infty}^{\infty} w(x-x') H\left(u\left(x', t - \frac{|x-x'|}{v}\right) - \theta\right) dx',$$

where $v > 0$ represents the axonal conduction velocity and the firing rate is again described using the Heaviside function. Note that as axonal conduction time becomes instantaneous (i.e., $v \to \infty$), we return to the original formulation.

Assuming a traveling front solution oriented as above and expressed in terms of traveling coordinates, the equation becomes

$$-cU' + U = \int_{-\infty}^{\infty} w(z-z') H\left(U\left(z' + \frac{c|z-z'|}{v}\right) - \theta\right) dz'.$$

The right-hand side simplifies to

$$f(z) = \begin{cases} \frac{1}{2} & \text{if } c > v, \\ \int_{\frac{v}{v-c}z}^{\infty} w(y)dy & \text{if } v \geq c \geq -v, \\ \int_{-\infty}^{\frac{v}{v+c}z} w(y)dy + \int_{\frac{v}{v-c}z}^{\infty} w(y)dy & \text{if } c < -v, \end{cases}$$

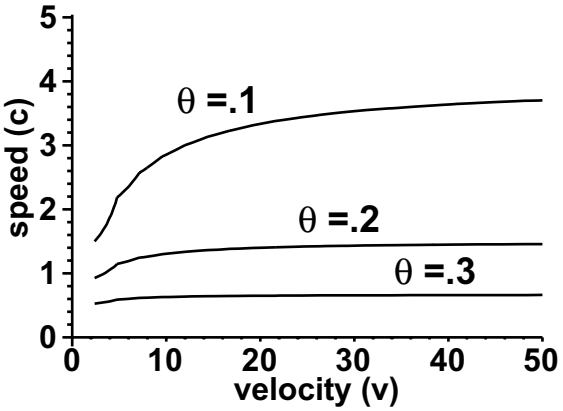

FIG. 4. *Effect on wave speed of axonal conduction velocity. The relationship between wave speed (c) and velocity (v) is described by* $\theta = \int_0^\infty e^{-s} \int_{\frac{cvs}{v-c}}^\infty w(x)dxdt$, *where* $w(x) = \frac{e^{-1/(2x^2)}}{\sqrt{2\pi}}$, *and* $\theta = .1, .2, .3$. *Note that axonal velocity has a negligible effect on wave speed except when* $v \approx c$. *(Note also the different scales of the c and v axes.)*

and we obtain an implicit function of wave speed proceeding as in [18],

$$U' - \frac{1}{c}U = -\frac{1}{c}f(z),$$
$$U(\xi) = e^{\xi/c}\left(\theta - \frac{1}{c}\int_0^\xi e^{-z/c}f(z)dz\right).$$

Now, since the traveling front solution $U(\xi)$ is bounded as $\xi \to \pm\infty$, it must be that

$$\theta = \frac{1}{c}\int_0^\infty e^{-\frac{z}{c}}f(z)dz.$$

Thus wave speed and axonal velocity relate according to

$$\theta = \int_0^\infty e^{-s}f(cs)ds,$$

where $f(z)$ is as above. Note that only the portion in which $v \geq c \geq -v$ is physiologically relevant since wave speed cannot exceed conduction velocity, and that a discontinuity occurs in the relationship just at this point.

A numerical example of this relationship is shown in Figure 4. Note that axonal velocity has a negligible effect on wave speed except when $v - c \approx 0$. Experimentally, the propagation of an action potential along a cortical axon is found to be roughly 2–4 m/s [52], two orders of magnitude faster than the measured wave speed (20–100 mm/s) [7]. This provides justification for the assumption of infinite conduction velocity implicit in (2).

2.2.3. Wave speed and synaptic parameters. With a slight modification to (2), we reformulate the system to express the influence of ionic and synaptic currents on neuronal activity,

$$u_t(x,t) = g_L(u_L - u) + g_{syn}\left(\int_{-\infty}^\infty w(x-x')H(u(x',t)-\theta)dx'\right)(u_{syn} - u),$$

where g_L and g_{syn} represent leak and synaptic conductances, u_L and u_{syn} are the leak and synaptic reversal potentials, and the remaining active currents have been absorbed into the firing rate function, which we again take to be $H(u-\theta)$ (see [14]). Note that the existence of traveling front solutions for equations of this form are covered by the results of [6].

Without loss of generality let $u_L = 0$. Front solutions, $u(x,t) = U(x-ct)$, in traveling coordinates, $z = x - ct$, then satisfy

$$\begin{aligned} -cU'(z) &= -g_L U + g_{syn}\left(\int_{-\infty}^{0} w(z-z')dz'\right)(U_{syn}-U) \\ &= -\left(g_L + g_{syn}\int_z^{\infty} w(y)dy\right)U + g_{syn}U_{syn}\int_z^{\infty} w(y)dy. \end{aligned}$$

To simplify, define the *total conductance* $g_T(z)$ as

$$g_T(z) = g_L + g_{syn}\int_z^{\infty} w(y)dy,$$

so that

$$-cU'(z) + g_T(z)U = g_{syn}U_{syn}\int_z^{\infty} w(y)dy.$$

Solving for $U(z)$ and evaluating at $z = 0$ with substitutions similar to the above, we obtain

$$\begin{aligned} U(z) &= \frac{g_{syn}U_{syn}}{c}\int_0^{\infty} e^{-\frac{1}{c}\int_0^{cr-z} g_T(p+z)dp}\int_{cr}^{\infty} w(y)dydr, \\ \theta &= g_{syn}U_{syn}\int_0^{\infty} e^{-\frac{1}{c}\int_0^{cr} g_T(p)dp}\int_{cr}^{\infty} w(y)dydr. \end{aligned}$$

The result is a relationship with the same form as (5). Namely,

$$\theta = g_{syn}U_{syn}\int_0^{\infty}\alpha(q)\int_{cq}^{\infty} w(y)dydq,$$

where, in this case,

$$\alpha(q) = e^{-\frac{1}{c}\int_0^{cq} g_T(p)dp}.$$

Note that changes to U_{syn} are equivalent to rescaling the threshold, θ. Also, in addition to rescaling the threshold, g_{syn} affects the time course of activity in that it is included in the term for total cell conductance, g_T.

2.2.4. Numerical comparisons. The wave speed analysis described above can be compared to those same speeds determined by solving (2) numerically. This permits an investigation of wave speeds using more general activation functions for which the analysis is less straightforward. Figure 5 demonstrates the relationship between wave speed and threshold determined analytically from (5) as compared with numerically solving (2) using the same parameter values. A similar relation is found if the activation function is taken to be either piecewise linear or sigmoidal. (See Appendix for methods.)

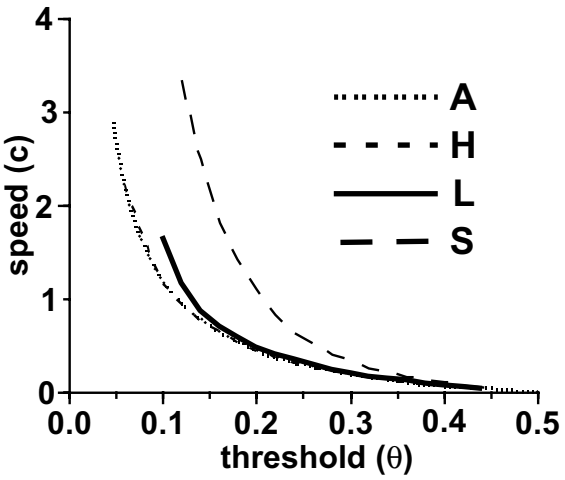

FIG. 5. *Wave speed as a function of threshold for a spectrum of activation functions. Wave speeds are computed from solutions to* $u_t + u = \int_{-\infty}^{\infty} \frac{1}{2(.3)} e^{-|y|/.3} P(u(y,t) - \theta) dy$. (A) *Analytically determined speed when* $P(u-\theta) = H(u-\theta)$ *(i.e., solving* (5)*).* (H) *Numerically determined speed when* $P(u-\theta) = H(u-\theta)$. (L) *Numerically determined speed when* P *is piecewise linear, i.e.,* $P(U) = 0$ *for* $(U-\theta) < (-1/12), .5+6(U-\theta)$ *for* $(-1/12) \le (U-\theta) \le (1/12), 1$ *for* $(U-\theta) > (1/12)$. (S) *Numerically determined speed when* P *is sigmoidal but with the same linear slope as L, i.e.,* $P(u-\theta) = (1/2)(1+\tanh(6(u-\theta)))$. *Note that the nonlinear portion of the sigmoid has a substantial effect on wave speed at lower thresholds.*

Interestingly, compared to a piecewise linear function, sigmoidal firing rate functions generate waves of much higher speed for a given threshold, indicating that the nonlinear portion of the activation function has a significant effect on activity propagation. This makes intuitive sense in that the gradual decline of a sigmoid function allows for some amount of network activity to be generated even at low-average voltage levels. (See [44] for discussion.)

3. Traveling pulses. We present two strategies for constructing traveling pulse solutions to (3), i.e., solutions of the form $u(x,t) = U(x-ct)$, $U(\pm\infty) = 0$, $U(0) = U(a) = \theta$, $0 < \theta < 1/2$, $c < 0$, $a > 0$ (see Figure 6). The first approach describes the firing rate using the Heaviside function, enabling a reduction of the system to an ODE with interior conditions and conditions at $\pm\infty$. The second assumes a firing rate function of a more general form and exploits the difference in time scales introduced by the slow negative feedback to construct a pulse using singular perturbation methods.

3.1. Reduction to an ODE and shooting. With the assumption that the decay of negative feedback is weak (i.e., $\beta = 0$), and taking the Heaviside function to describe firing rate, (3) expressed in traveling coordinates becomes

$$\begin{aligned} -cU' + U &= \int_{-\infty}^{\infty} w(z-z') H(U(z') - \theta) dz' \quad - V, \\ -cV' &= \epsilon U. \end{aligned}$$

Note that, in the following calculations, we need not assume ϵ is small.

With the pulses aligned such that $c < 0$, the system is reduced as follows:

$$-cU' + U = \int_0^a w(z-z') dz' - V,$$

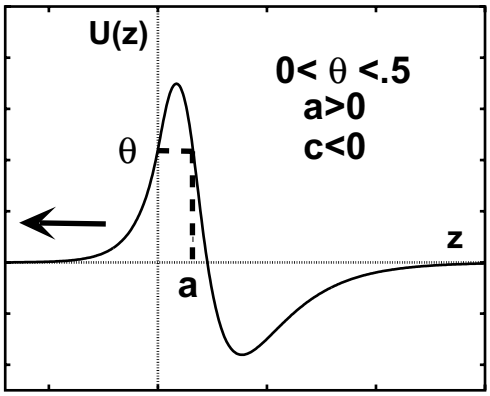

FIG. 6. *Description of the traveling pulse solution in traveling coordinates.*

$$-cV' = \epsilon U,$$

or

$$\begin{aligned} -cU' + U &= \int_{z-a}^{z} w(y)dy - V, \\ -cV' &= \epsilon U. \end{aligned}$$

Differentiating the first equation and substituting in the second, we obtain a second order ODE with conditions along the interior and at $\pm\infty$:

$$\left\{ \begin{array}{rcl} -c^2U'' + cU' - \epsilon U &=& c(w(z) - w(z-a)), \\ U(0) = U(a) &=& \theta, \\ U(\pm\infty) &=& 0. \end{array} \right. \tag{6}$$

Thus, for the existence of traveling pulse solutions to (3), it suffices to determine values of $c < 0$ and $a > 0$ such that (6) has a solution.

One strategy for determining such values is to examine solutions to (6) along different regions of the real axis that also satisfy certain matching conditions at their junctions. For $z \leq 0$, (6) becomes a boundary value problem with conditions $U(0) = \theta$, $U(-\infty) = 0$. The solution, U^-, provides a constraint on the relationship between a and c.

To illustrate the strategy, we consider the case in which $w(z) = e^{-|z|}/2$ $(z \leq 0)$. A subsequent report will investigate solutions arising from more general weight kernels (D.J. Pinto and C.E. Wayne, in preparation).

$$\left\{ \begin{array}{rcl} -c^2U'' + cU' - \epsilon U &=& \frac{c}{2}(e^z - e^{z-a}), \\ U(0) &=& \theta, \\ U(-\infty) &=& 0. \end{array} \right.$$

Here, the solution can be found explicitly, namely, $U^-(z) = \theta e^z$ $(z \leq 0)$.

Substituting this back into (6) yields

$$-c^2\theta e^z + c\theta e^z - \epsilon\theta e^z = \frac{c}{2}e^z(1 - e^{-a}),$$

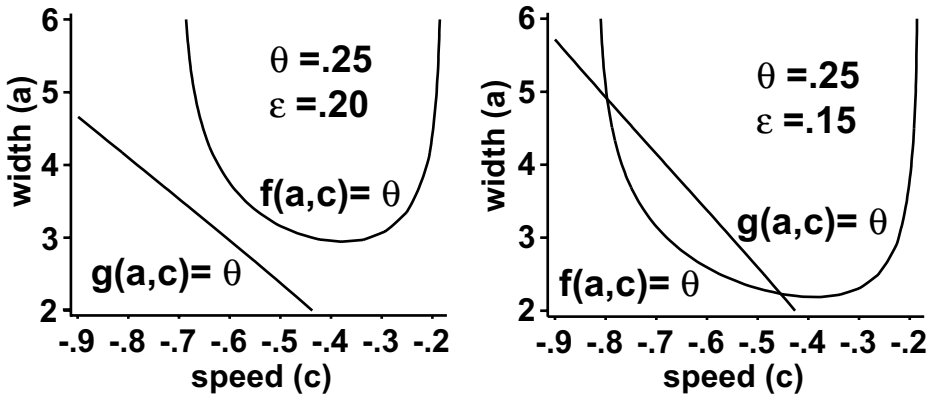

FIG. 7. *Relationship between speed* (c) *and pulse width* (a). $f(a,c)$ *was determined analytically by considering solutions to* (6) *on* $[0,-\infty)$. $g(a,c)$ *was described numerically by fixing* c *at different values and taking* a *as a shooting parameter to satisfy the same equation on* $[0,\infty)$. *Values of* a *and* c *which satisfy both relationships denote traveling pulse solutions of* (5) *over the entire real axis.*

which specifies a relationship that appropriate values of c and a must satisfy,

$$\theta = f(a,c) = \frac{c(1-e^{-a})}{2(-c^2+c-\epsilon)}.$$

For $z \geq 0$, (6) represents a second boundary value problem with conditions $U(0) = \theta$, $U(\infty) = 0$, and the interior condition $U(a) = \theta$. Note that as $z \to \infty$, $w(z) \to 0$, and solutions approach those of the homogeneous system, all of which tend to zero. Thus the condition at $+\infty$ follows naturally. In addition, in order to match the solution from the first problem, we require $U'(0) = U^{-'}(0)$ (θ, in the above example). The solution to this second problem, $U^+(z)$, provides another constraint on the relationship between c and a.

Using the above example, we can again explicitly produce the solution U^+ as well as the second relationship $g(c,a) = \theta$. Alternately, the relationship can be determined numerically by fixing $c < 0$ and considering a as a shooting parameter to solve the boundary value problem.

A full solution to (6), then, can be found for just those values of c and a which satisfy both $f(a,c) = \theta$ and $g(a,c) = \theta$. The two conditions also provide both the speed and width of pulse solutions to the original problem (3).

Figure 7 shows the plots of both $f(a,c)$ and $g(a,c)$ for the example problem described above. With slow negative feedback (ϵ small) there are, in fact, two pulse solutions, one narrow and slow and the other wide and fast. As ϵ increases and feedback becomes more rapid, the solutions converge and vanish. The same behavior is observed when varying the firing threshold θ (not shown). A similar pair of pulses arises in the reaction-diffusion system studied in [50]. As was found in that case, it is likely that stability analysis will confirm our numerical results that reveal the larger, fast pulse to be stable, while the narrow, slow pulse is unstable. Figure 8 illustrates the two pulses satisfying the problem when negative feedback is slow.

3.2. Singular perturbation construction. Returning to (3), we now consider the general class of firing rate functions, $P(u)$, that are continuous and nonlinear. Exploiting the second time scale introduced by slow negative feedback, as well as the existence of front solutions from [18], we construct a traveling pulse solution using

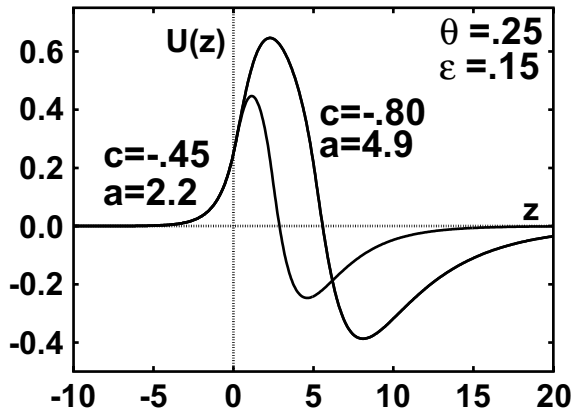

FIG. 8. *Examples of two pulse solutions which satisfy* (5).

singular perturbation techniques. The strategy is similar to the construction of pulses in a reaction-diffusion system but is complicated by the lack of a closed form expression for the leading and trailing fronts.

Expressed in traveling coordinates, (3) takes the form

$$\begin{aligned} -cU' &= -U + \int_{-\infty}^{\infty} w(z-z')P(U(z')-\theta)dz' - V, \\ -cV' &= \epsilon(-\beta V + U). \end{aligned}$$

We analyze separately the fast and slow time behavior.

In fast time, the slow feedback is taken as essentially constant ($\epsilon = 0$). This leads to the fast time, or inner layer equations,

$$\begin{aligned} -cU' &= -U + \int_{-\infty}^{\infty} w(z-z')P(U(z')-\theta)dz' - V_0, \\ V' &= 0 \qquad\qquad\qquad (V \equiv V_0). \end{aligned}$$

In slow time, we compress the z-axis with the change of variable $\xi = \epsilon z$,

$$\begin{aligned} -c\epsilon U_\xi &= -U + \int_{-\infty}^{\infty} \frac{1}{\epsilon} w((\xi-\xi')/\epsilon)P(U(\xi')-\theta)d\xi' - V \\ -cV_\xi &= -\beta V + U, \end{aligned}$$

so that, as $\epsilon \to 0$, the fast variable, U, becomes essentially instantaneous. Also, for a Gaussian-like kernel such as w, as $\epsilon \to 0$

$$\frac{1}{\epsilon} w\left(\frac{(\xi-\xi')}{\epsilon}\right) \to \delta(\xi).$$

From the first equation, then, we obtain

$$V = -U + P(U(\xi) - \theta),$$

while the second expression yields the slow time, or outer layer equations

$$V_\xi = \frac{1}{c}(\beta V - U) = \frac{1}{c}(\beta V - g_\pm(V)),$$

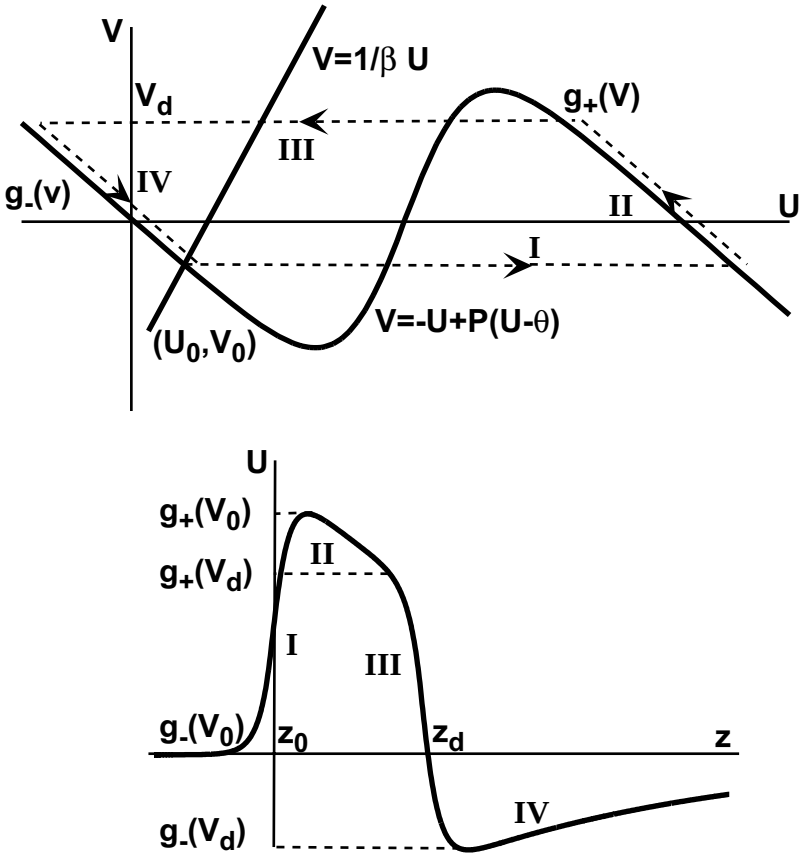

FIG. 9. *Illustration of the singular perturbation construction process using the phase-plane and in traveling coordinates.*

where $g_\pm(V)$ describes U as a function of V along the appropriate branch of $(-U + P(U-\theta))^{-1}$ (see Figure 9).

The phase-plane for the space-clamped system is useful for illustrating the construction process (see Figure 9). We assume β is small enough to avoid the situation of local bistability. The strategy is to progressively gather solutions to the equations from each layer and assemble them by matching their values at each junction. Note also that, in contrast to the shooting argument presented above, only one pulse solution is obtained using singular perturbation techniques. This is to be expected, however, in that as ϵ is decreased, the narrow pulse in the previous section becomes more narrow and ultimately vanishes as $\epsilon \to 0$ (see Figure 7) .

From the initial rest state (U_0, V_0), we use the fast, inner equations and apply the existence results of [18] to obtain a leading front solution at location z_0 with speed c_0 and matching conditions $\lim_{z\to\pm\infty} U(z) = g_\pm(V_0)$ (I). For $z > z_0 + O(\epsilon)$, the slow outer equation $cV_\xi = (\beta V - g_+(V))$ governs the plateau solution (II). Note that, as $g_+(V) > V$ and, in this case, $c < 0$, we have $V_\xi > 0$, so V increases along the upper branch.

With V increasing, the solution must leave the $g_+(V)$ branch at some point, V_d. Here, the inner equations are again used to construct a trailing back at location

z_d with matching conditions $\lim_{z\to\pm\infty}U(z) = g_{\mp}(V_0)$ (III). The drop value, V_d, is determined such that the speed of the back matches that of the front, ensuring that the pulse retains its shape as it travels (see below).

Beyond $z_d + O(\epsilon)$, the outer equation $V_\xi = \frac{1}{c}(V - g_-(V))$ is employed to produce the recovery stage, bringing the solution back to rest (IV). Note that, as $g_-(V) < V$, V decreases along the $g_-(V)$ branch.

It remains to establish the existence of some value for V_d along the $g_+(V)$ branch for which the speed of the trailing back matches that of the leading front. To this end, we first determine the dependence of wave speed on the value of V.

At each point V_p along the $g_+(V)$ branch, we proceed from the inner equation,

$$-cU' = -U + \int_{-\infty}^{\infty} w(z - z')P(U(z') - \theta)dz' - V_p$$

to obtain a traveling front solution, U_p, with $\lim_{z\to\pm\infty}U(z) = g_{\mp}(V_p)$. An identical argument to that presented by [18] shows that the speed, c_p, of this front satisfies

$$c_p = \frac{-\int_{g_-(V_p)}^{g_+(V_p)}(-U - V_p + P(U - \theta))dU}{\int_{-\infty}^{\infty}(U')^2P'(U - \theta)dz}.$$

Note that, as the denominator is strictly positive (recall that P is monotonically increasing), c_p has the same sign as $\int(P(U - \theta) - (U + V_p))dU$. This provides the necessary insight into the dependence of wave speed on V. As illustrated in Figure 10, during the plateau phase, as V increases from V_0 to V_d, the value of the integral, and hence the potential trailing back speed c_p, increases and ultimately changes sign.

This relationship further indicates that the range of possible values for c_p, in particular, whether it is possible to attain $c_p = -c_0$, depends on the profile of U and the shape of $P(U - \theta)$. In the case of certain reaction-diffusion systems, the solution U, and hence the wave speed c, can be expressed in closed form, making the determination of possible wave speeds a straightforward matter [55], [23]. In the present system, it remains unclear if a closed form solution is possible except in special cases. However, the existence of a matching speed for the trailing back can be determined with further assumptions on the shape of the activation function.

In particular, suppose that the sigmoidal activation function P is odd-symmetric about its inflection point. We choose a coordinate frame such that the origin is situated at that point (see Figure 10) and such that

1. $P(-(U - \theta)) = -P(U - \theta)$,
2. $\int_{g_-(V)}^{g_+(V)} P(U - \theta) - (U + V)dU = 0$ just when $V = 0$,
3. $g_{\pm}(-V) = -g_{\mp}(V)$,

all of which follow directly from the symmetry assumptions on P. For example, $P(U) = \frac{1}{2}(1 + \tanh(\beta(U - \theta)))$ satisfies these conditions.

Given V_0 ($V_0 < 0$, say), let U_f be the front solution satisfying the boundary and matching conditions

$$\begin{cases} -cU_f' &= -U_f + \int_{-\infty}^{\infty} w(z - z')P(U_f(z') - \theta)dz' - V_0, \\ \lim\limits_{z\to\pm\infty} U_f &= g_{\pm}(V_0). \end{cases}$$

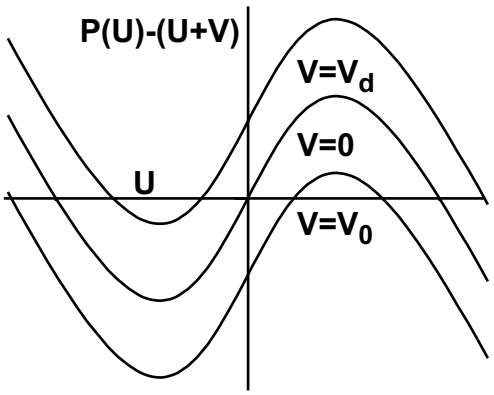

FIG. 10. *Relationship of wave speed to the level of negative feedback (V). As the value for V moves from V_0 to V_d, the value of $\int(P(U)-(U+V))dU$ increases and eventually changes sign. With assumptions on the symmetry of P, we can guarantee a value for V_d which yields a speed equal to but opposite that obtained from V_0.*

Since V_0 lies in the domain of g_-, condition 3 says that $V_d = -V_0$ lies in the domain of g_+. Thus we have U_d, which we take as the trailing back solution, satisfying

$$\begin{cases} -cU_d' &= -U_d + \int_{-\infty}^{\infty} w(z-z')P(U_d(z')-\theta)dz' - V_d, \\ \lim\limits_{z\to\pm\infty} U_d &= g_{\mp}(V_d). \end{cases}$$

Finally, with the three properties listed, it is easy to show that the function $-U_f$ also satisfies these trailing back conditions, and we conclude, by uniqueness, that $-U_f = U_d$. Thus the profile of the trailing back is simply a reversed, shifted version of the front with equal but opposite velocity.

In [5], a similar symmetry argument is used to obtain an appropriate trailing back solution to the Fitzhugh–Nagumo equations. More generally, however, it may happen that, as V increases along the $g_+(V)$ branch, the cusp of the sigmoid is encountered before a drop point is found for which the back speed matches that of the front. In reaction-diffusion systems, trailing back solutions still exist at such points but are no longer unique. It is straightforward to show, in fact, that such situations admit a family of fronts with arbitrary speed subject only to some minimum value. Such solutions have been referred to as "phase waves," while those arising from the regions of bistability along the interior of the sigmoid are called "trigger" waves (see [55] for review). Phase waves have been shown, most recently in [51], to exhibit shapes and speeds which depend on initial conditions rather than the diffusion term and, in some cases, which vary as a function of time. For the convolution equations discussed here, the situation leading to phase waves has not yet been fully examined, though some nonexistence results have been established under certain conditions [11].

4. Discussion. This study investigates traveling front and pulse solutions to equations that describe spatially distributed and synaptically coupled neural networks. Using a simple, yet biophysically motivated set of equations, a relationship is established between the experimental measure of propagation speed and various network features such as neuronal threshold, synaptic parameters, and axonal distribution. The addition of a slow local negative feedback term to the equations results in solutions best described as traveling pulses. With limiting assumptions on

the local dynamics, the problem of existence is reduced to finding any solution to a set of boundary value problems, accomplished using a shooting-type argument. For more general dynamics, the difference in time scales between fast excitation and slow negative feedback allows for the construction of asymptotic approximations to pulse solutions using a singular perturbation approach.

In contrast to the propagation of activity down axons of individual neurons, which is mediated by diffusion, activity propagation through a neuronal network is thought to be synaptic in origin. Recent large scale computational models have provided important insights into the operation of such networks [26], [3]. Numerically, synaptically-coupled networks have been shown to exhibit oscillating and propagating waves (see [9], [35]) as well as both transient [59] and persistent behaviors [4]. Analytically, the emergence of spatial activity structures has been established under certain conditions (see [2], [20], [17]), and the existence of traveling front solutions has been verified under more general circumstances [18], [11] (see [13] for review).

Much of the above analysis is motivated both by experimental findings in the cortex and by the example set by previous studies on diffusively coupled systems. Examined extensively in the form of the reaction-diffusion equations, traveling fronts (see [37], [22], [21]), pulses (see [5], [30], [29]), standing patterns (see [16], [53]), and other spatial structures [60], [36] (see [55] for review) have each been analytically demonstrated to exist as solutions.

While diffusive coupling is appropriate only for a specialized set of network processes (e.g., electrical coupling), the strategies that have been developed to analyze the equations remain quite relevant. Indeed, if the analytic development of reaction-diffusion systems is any indication, the present results represent only a sampling of the analysis that might be conducted. Besides fronts and pulses, pulse-train solutions (see [29], [34], [48], [31]), solutions in bistable media [49], mechanisms for nonuniform propagation (see [47], [19]), and the transition from standing to traveling solutions (see [43], [41]) have each been developed in the reaction-diffusion literature with techniques that may be readily adapted to synaptically couped networks. With the cortex more properly modeled as a two-dimensional structure, spiral waves (see [27], [36], [42]), target patterns (see [28], [36]), and other spatial structures [53] also become possible.

Appendix. Methods. The techniques for preparing cortical slices are essentially the same as those described previously by others [7]. Briefly, Sprague–Dawley rats aged 4–7 weeks were deeply anaesthetized with metofane (methoxyflurane, Pitman–Moore, Mundelein, IL). The rats were decapitated, their brains were removed, and 400 μm-thick slices through somatosensory cortex (SmI) were made in a plane corresponding to the thalamocortical fiber pathway [1]. Slices were transferred to a room temperature fluid/gas interface chamber, saturated with humidified 95% O_2-5% CO_2, and bathed with artificial cerebrospinal fluid (ACSF). Following the experiments, slices were fixed overnight in 4% paraformaldehyde and stained with cytochrome oxidase using a standard histological technique.

For electrophysiological recording, slices were maintained at 34^oC, bathed in ACSF, and bicuculline methiodide (20 μm) was added to the bathing solution to induce propagating epileptiform activity. The thalamocortical fiber tract was severed to ensure that observed activity was strictly cortical in origin. Extracellular field potential recordings were obtained using an electrode array specifically constructed for these experiments. The array consisted of 16 stainless steel microwires (25 μm diameter, California Fine Wire Co.) spaced 100 μm apart, for a total span of 1.6

mm. The array was positioned along cortical layer II/III parallel to the pial surface. Waves were initiated using an electrical stimulus (200 μs, 10-100 μA) applied through a concentric bipolar stimulating electrode positioned several millimeters lateral to the recording array.

All numerical simulations were written specifically for this study using standard C and compiled with gcc. Convolution integrals were evaluated using the trapezoidal method with $\Delta x = .1$. Derivatives were computed using a fourth-order Runge–Kutta method with $\Delta t = .1$. Smaller grid sizes were examined to ensure the stability of numerical solutions. Pulse speed was determined by noting the time at which activity reached half-maximum at two different points in the domain. Data were plotted using Origin software and arranged using Canvas 6.0. Phase planes were created using the XPP software package [15] and Maple 6.0 (Waterloo Software).

Acknowledgments. The authors wish to acknowledge Tasso Kaper and Eugene Wayne for their useful comments and criticisms, and Barry Connors for the use of his laboratory in conducting the experiments.

REFERENCES

[1] A. Agmon, B. W. Connors, *Thalamocortical responses of mouse somatosensory (barrel) cortex in vitro*, Neurosci., 41 (1991), pp. 365–379.

[2] S. Amari, *Dynamics of pattern formation in lateral-inhibition type neural fields*, Biol. Cybernet., 27 (1977), pp. 77–87.

[3] P. C. Bressloff, *Traveling waves and pulses in a one-dimensional network of excitable integrate-and-fire neurons*, J. Math. Biol., 40 (2000), pp. 169–198.

[4] M. Camperi and X. J. Wang, *A model of visuospatial short-term memory in prefrontal cortex: Cellular bistability and recurrent network*, J. Comput. Neurosci., 5 (1998), pp. 383–405.

[5] R. G. Casten, H. Cohen, and P. A. Lagerstrom, *Perturbation analysis of an approximation to the Hodgkin-Huxley theory*, Quart. Appl. Math., 32 (1975), pp. 365–402.

[6] Z. Chen, G. B. Ermentrout, and B. McLeod, *Traveling fronts for a class of non-local convolution differential equations*, Appl. Anal., 64 (1997), pp. 235–253.

[7] R. D. Chervin, P. A. Pierce, and B. W. Connors, *Periodicity and directionality in the propagation of epileptiform discharges across neocortex*, J. Neurophysiol., 60 (1988), pp. 1695–1713.

[8] B. W. Connors and Y. Amitai, *Generation of epileptiform discharge by local circuits of neocortex*, in Epilepsy: Models, Mechanisms, and Concepts, P. A. Schwartkroin, ed., Cambridge University Press, Cambridge, UK, 1993, pp. 388–423.

[9] A. Destexhe, T. Bal, D. A. McCormick, and T. Sejnowski, *Ionic mechanisms underlying synchronized oscillations and propagating waves in a model of ferret thalamic slices*, J. Neurophysiol., 76 (1996), pp. 2049–2070.

[10] E. A. DeYoe, P. Bandettini, J. Neitz, D. Miller, and P. Winans, *Functional magnetic resonance imaging (FMRI) of the human brain*, J. Neurosci. Meth., 54 (1994), pp. 171–187.

[11] O. Diekman and H. G. Kaper, *On the bounded solutions of a nonlinear convolution equation*, Nonlinear Anal., 2 (1978), pp. 721–737.

[12] G. B. Ermentrout, *The analysis of synaptically generated traveling waves*, J. Comput. Neurosci., 5 (1998), pp. 191–208.

[13] G. B. Ermentrout, *Neural nets as spatio-temporal pattern forming systems*, Rep. Progr. Phys., 61 (1998), pp. 353–430.

[14] G. B. Ermentrout, *Reduction of conduction-based models with slow synapses to neural nets*, Neural Comp., 6 (1994), pp. 679–695.

[15] G. B. Ermentrout, *XPP-X Windows dynamical systems software*, http://www.pitt.edu/phase, 1994.

[16] G. B. Ermentrout, *Stripes or spots? Nonlinear effects in bifurcation of reaction-diffusion equations on the square*, Proc. Roy. Soc. London A, 434 (1992), pp. 413–417.

[17] G. B. Ermentrout, *Asymptotic behavior of stationary homogeneous neuronal nets*, in Competition and Cooperation in Neural Nets, Springer-Verlag, New York, 1982, pp. 57–70.

[18] G. B. Ermentrout and J. B. McLeod, *Existence and uniqueness of traveling waves for a neural network*, Proc. Roy. Soc. Edinburgh Sect. A, 123 (1993), pp. 461–478.

[19] G. B. Ermentrout and J. Rinzel, *Reflected waves in an inhomogeneous excitable medium*, SIAM J. Appl. Math., 56 (1996), pp. 1107–1128.
[20] G. B. Ermentrout and J. D. Cowan, *Large scale spatially organized activity in neural nets*, SIAM J. Appl. Math., 38 (1980), pp. 1–22.
[21] P. C. Fife and J. B. McLeod, *A phase plane discussion of convergence to traveling fronts for nonlinear diffusion*, Arch. Rational Mech. Anal., 75 (1981), pp. 281–314.
[22] P. C. Fife and J. B. McLeod, *The approach of solutions of nonlinear diffusion equations to traveling front solutions*, Arch. Rational Mech. Anal., 65 (1977), pp. 335–361.
[23] P. C. Fife, *Mathematical Aspects of Reacting and Diffusing Systems*, Lecture Notes in Biomath. 28, Springer-Verlag, Berlin, 1979.
[24] W. Gerstner, *Time structure of the activity in neural-network models*, Phys. Rev. E(3), 51 (1995), pp. 738–758.
[25] C. D. Gilbert and T. N. Wiesel, *Columnar specificity of intrinsic horizontal and corticocortical connections in cat visual cortex*, J. Neurosci., 9 (1989), pp. 2432–2442.
[26] D. Golomb and Y. Amitai, *Propagating neuronal discharges in neocortical slices: Computational and experimental study*, J. Neurophysiol., 78 (1997), pp. 1199–211.
[27] P. S. Hagan, *Spiral waves in reaction-diffusion equations*, SIAM J. Appl. Math., 42 (1982), pp. 762–786.
[28] P. S. Hagan, *Target patterns in reaction-diffusion systems*, Adv. in Appl. Math., 42 (1981), pp. 400–416.
[29] S. P. Hastings, *Single and multiple pulse waves for the Fitzhugh–Nagumo equations*, SIAM J. Appl. Math., 42 (1982), pp. 247–260.
[30] S. P. Hastings, *On the existence of homoclinic and periodic orbits for the Fitzhugh–Nagumo equations*, Quart. J. Math. Oxford Ser. (2), 27 (1976), pp. 123–134.
[31] L. N. Howard and N. Kopell, *Wave trains, shock fronts, and transition layers in reaction-diffusion equations*, in Mathematical Aspects of Chemical and Biochemical Problems and Quantum Chemistry, Proceedings of the SIAM–AMS Symposium on Applied Mathematics, New York, SIAM, Philadelphia, AMS, Providence, RI, 1974, pp. 1–12.
[32] D. Hubel and T. Weisel, *Receptive fields and functional architecture of monkey striate cortex*, J. Physiol., 195 (1968), pp. 215–243.
[33] M. A. P. Idiart and L. F. Abbott, *Propagation of excitation in neural network models*, Networks, 4 (1993), pp. 285–294.
[34] J. P. Keener, *Waves in excitable media*, SIAM J. Appl. Math., 39 (1980), pp. 528–548.
[35] N. Kopell and G. B. Ermentrout, *Symmetry and phaselocking in chains of weakly coupled oscillators*, Comm. Pure Appl. Math., 39 (1986), pp. 623–660.
[36] N. Kopell and L. N. Howard, *Target pattern and spiral solutions to reaction-diffusion equations with more than one space dimension*, Adv. in Appl. Math., 2 (1981), pp. 417–449.
[37] N. Kopell and L. N. Howard, *Plane wave solutions to reaction-diffusion equations*, Stud. Appl. Math., 52 (1973), pp. 291–328.
[38] B. Lancaster and P. R. Adams, *Calcium-dependent current generating the afterhyperpolarization of hippocampal neurons*, J. Neurophys., 55 (1986), pp. 1268–82.
[39] J. W. Lance, *Current concepts of migraine pathogenesis*, Neurology, 43 (1993), pp. S11–S15.
[40] R. Miles, R. D. Traub, and R. K. S. Wong, *Spread of synchronous firing in longitudinal slices from the CA3 region of the hippocampus*, J. Neurophysiol., 60 (1995), pp. 1481–1496.
[41] V. V. Osipov, *Criteria of spontaneous interconversions of traveling and static arbitrary dimensional dissipative structures*, Phys. D, 93 (1996), pp. 143–156.
[42] J. Paullet, G. B. Ermentrout, and W. Troy, *The existence of spiral waves in an oscillatory reaction-diffusion system*, SIAM J. Appl. Math., 54 (1994), pp. 1386–1401.
[43] D. M. Petrich and R. E. Goldstein, *Nonlocal contour dynamics model for chemical front motion*, Phys. Rev. Lett., 72 (1994), pp. 1120–1123.
[44] D. J. Pinto, J. C. Brumberg, D. J. Simons, and G. B. Ermentrout, *A quantitative population model of whisker barrels: Re-examining the Wilson-Cowan equations*, J. Comput. Neurosci., 3 (1996), pp. 247–264.
[45] J. C. Prechtl, L. B. Cohen, B. Pesaran, P. P. Mitra, and D. Kleinfeld, *Visual stimuli induce waves of electrical activity in turtle cortex*, Proc. Natl. Acad. Sci., 94 (1997), pp. 7621–7626.
[46] W. Rall, *Cable theory for dendritic neurons*, in Methods in Neuronal Modeling, C. Koch and I. Segev, eds., MIT Press, Cambridge, MA, 1989, pp. 9–62.
[47] J. Rinzel, *Mechanisms for nonuniform propagation along excitable cables*, in Mathematical Approaches to Cardiac Arrhythmias, Ann. New York Acad. Sci. 591, Acad. Sci. New York, New York, 1990, pp. 51–61.

[48] J. Rinzel, *Impulse propagation in excitable systems*, in Dynamics and Modeling of Reactive Systems, C. W. E. Stewart et al., eds., Academic Press, New York, 1979, pp. 259–291.
[49] J. Rinzel and D. Terman, *Propagation phenomena in a bistable reaction-diffusion system*, SIAM J. Appl. Math., 42 (1982), pp. 1111–1137.
[50] J. Rinzel and J. B. Keller, *Traveling wave solutions of a nerve conduction equation*, Biophys. J., 13 (1973), pp. 1313–1337.
[51] J. A. Sherratt and B. P. Marchant, *Algebraic decay and variable speeds in wavefront solutions of a scalar reaction-diffusion equation*, IMA J. Appl. Math., 56 (1996), pp. 289–302.
[52] H. A. Swadlow, *Efferent neurons and suspected interneurons in SI forelimb representation of the awake rabbit: Receptive fields and axonal properties*, J. Neurophysiol., 63 (1990), pp. 1477–1498.
[53] T. Takaishi, M. Mimura, and Y. Nishiura, *Pattern formation in coupled reaction-diffusion systems*, Japan J. Indust. Appl. Math., 12 (1995), pp. 385–424.
[54] R. D. Traub, J. G. Jefferys, and R. Miles, *Analysis of the propagation of disinhibition-induced after-discharges along the guinea-pig hippocampal slice in vitro*, J. Physiology, 472 (1993), pp. 267–287.
[55] J. J. Tyson and J. P. Keener, *Singular perturbation theory of traveling waves in excitable media: A review*, Phys. D, 32 (1988), pp. 327–361.
[56] C. von der Malsburg, *Binding in models of perception and brain function*, Curr. Opin. Neurobiol., 5 (1995), pp. 520–526.
[57] C. Welker, *Microelectrode delineation of fine grain somatotopic organization of (SmI) cerebral neocortex in albino rat*, Brain Res., 26 (1971), pp. 259–275.
[58] E. L. White, *Cortical Circuits: Synaptic Organization of the Cerebral Cortex. Structure, Function and Theory*, Birkhäuser Boston, Boston, 1989.
[59] H. R. Wilson and J. D. Cowan, *A mathematical theory of the functional dynamics of cortical and thalamic nervous tissue* Kybernetika (Prague), 13 (1973), pp. 55–80.
[60] A. T. Winfree, *Wavelike activity in biological and chemical media*, in Mathematical Problems in Biology, P. van den Driessche, ed., Springer-Verlag, Berlin, 1974, pp. 241–260.
[61] J. Y. Wu, L. Guan, and Y. Tsau, *Propagating activation during oscillations and evoked responses in neocortical slices*, J Neurosci., 19 (1999), pp. 5005–5015.